Towards realistic radiofrequency ablation of hepatic tumors 3D simulation and planning

Caroline Villard[a], Luc Soler[b], Afshin Gangi[c], Didier Mutter[b] and Jacques Marescaux[b]

[a]LSIIT UMR 7005 CNRS – Université Louis Pasteur Strasbourg I,
Pôle API Boulevard S. Brant, F-67400 Illkirch, France;
[b]IRCAD, 1 place de l'Hôpital, F-67000 Strasbourg, France;
[c]Hôpital Civil, Service de Radiologie B, 1 place de l'Hôpital, F-67000 Strasbourg, France

ABSTRACT

Radiofrequency ablation (RFA) has become an increasingly used technique in the treatment of patients with unresectable hepatic tumors. Evaluation of vascular architecture, post-RFA tissue necrosis prediction, and the choice of a suitable needle placement strategy using conventional radiological techniques remain difficult. In an attempt to enhance the safety of RFA, a 3D simulator and treatment planning tool, that simulates the necrosis of the treated area, and proposes an optimal placement for the needle, has been developed. From enhanced spiral CT scans with 2 mm cuts, 3D reconstructions of patients with liver metastases are automatically generated. Virtual needles can be added to the 3D scene, together with their corresponding zones of necrosis that are displayed as a meshed spheroids representing the 60°C isosurface. The simulator takes into account the cooling effect of local vessels greater than 3mm in diameter, making necrosis shapes more realistic. Planned needle positioning can also be automatically generated by the software to produce complete destruction of the tumor, with maximum respect of the healthy liver and of all major structures to avoid. If he wishes, the radiologist can select on the skin an insertion window for the needle, focusing the research of the trajectory.

Keywords: minimally invasive surgery; treatment simulation and planning; computer-assisted surgery; 3D visualization

1. INTRODUCTION

Over the past 10 years, several minimally invasive techniques for liver tumor ablation have emerged thanks to recent advancements in medical imaging. Among them, percutaneous thermal ablation has been studied in different forms, such as microwave, laser, ultrasound, cryotherapy, and radiofrequency (RF) that appears to be the easiest, safest and most predictable.[1]

Radiofrequency is an ionic agitation generated by the principle of a microwave located at the tip of a needle-like probe, producing a tumor coagulative necrosis when heated enough. To treat a large zone, the probe may be positioned several times. Radiologists burn the whole tumor volume with a 0.5 to 1 cm security margin,[2] which is mandatory to prevent local recurrence of a tumor after treatment, and to reduce the effects of a possible inaccuracy of needle placement.

The success of such a treatment closely depends on the choice of secure probe trajectories, the destruction of a maximum number of cancerous cells, and a minimum amount of affected healthy tissues. Unfortunately, treatment planning is quite difficult for a radiologist who can only rely on 2D scanner slices.

New techniques of scanner image reconstruction allow a more intuitive 3D visualization of the patient's anatomy,[3] that makes the simulation of needle placement easier. The expected follow-ups of this functionality are both the visualization of the necrosis of treated zones, and the automatic planning of needle trajectories that would optimize the three above criteria.

In this paper, after a brief state of the art, we explain how we simulate the necrosis of the treated area. Then, we show how to automatically compute optimal needle position. Before concluding, we discuss the future enhancements we plan to add to improve radiofrequency ablation (RFA) treatment.

contact author : villard@lsiit.u-strasbg.fr

2. STATE OF THE ART

In radiofrequency treatment planning, recent studies bring us information about factors influencing lesion size and shape. Several kinds of factors are involved: device- or strategy-dependent, anatomic, or pathologic. Directly influencing the necrosis zone, they have to be taken into account for an accurate RFA simulation.

We know that the shape of the lesion depends on the type and design of probe, and its size varies according to the power supplied by the associated generator.[4] Furthermore, strategies can also help to overcome some problems due to anatomic properties, such as the *heat-sink* effect caused by blood flow inside vessel network. Blood supply occlusion allow to enlarge lesions, that are not disturbed by the heat-sink effect anymore.[5] And finally, some studies showed that the shape of lesions is not the same with cirrhotic/non-cirrhotic livers.[6]

On a technical point of view, very few studies have been carried out on treatment simulation and planning in the domain of radiofrequency. Most of them concerned other minimally invasive treatments such as cryotherapy,[7] and allowed to simulate iceball growth, or they were centered on finite elements modeling and did not seem to be real-time.[8] T. Butz proposed a very interesting cryotherapy simulator and planner, included in *3D-Slicer*, that can also be extended to one type of RF probe.[9] However, it can only compute the best positioning of cryoprobes within a predefined window of the body, and does not take into account the presence of surrounding organs.

3. METHODS

3.1. Visualizing the patient and simulating the necrosis zone

Our researches started with the expression of a need from radiologists to visualize more easily information about their patients, their anatomy and pathologies, and to be able to simulate accurately and realistically RF treatment before operating. Our tool, called *RF-Sim*, responds to these needs by linking 3D reconstruction of slices from an enhanced spiral CT scan,[3] 3D view of the patient, and virtual probe placement simulation and computation.

From enhanced spiral CT scans with 2 mm cuts, three dimensional (3D) reconstruction of patients with liver metastases are generated using a SGI octane2 under Unix with a R12000 processor at 400 MHz and 1Go of RAM. The dedicated software detects, delineates and reconstructs automatically their liver, pathologies, and surrounding organs. It produces realistic and manipulable 3D scenes representing the anatomy of the patients, in which it is possible to navigate easily, and to hide or show a selection of organs.

Then, simulations of RFA can be performed, based upon the characteristics of the Berchtold HITT needle. A user of the simulator can add virtual probes into the 3D scene of the patient's organs, as shown on Fig.1(a), and then freely translate and rotate them. During a simulation, for each attempt of needle placement, the corresponding lesion zone is estimated and simulated as a simple meshed spheroid representing the 60 °C isosurface.

The simulator is also able to take into account the cooling effect of local vessels greater than 3mm in diameter. To simulate this heat-sink effect induced by the vessels, we update the shape of the ellipsoid by repulsing some of its vertices away from the vessel shapes, towards the inside of the ellipsoid. Our deformation method, using a voxel representation of the vessel network and a voxel-based algorithm taking advantage of mathematical morphology techniques, as well as the obtained results are detailed in.[10] An example of necrosis shape deformation is shown on Fig.2. The deformation is computed in real-time while the user moves a needle or controls a lesion growth, to allow updates while needle is being adjusted. This is important as we want our prototype to be able to be run on every common laptop, to be brought in the operating room, and to be used live on location. This allows to observe whether the considered needle placement strategy would burn the whole cancerous zone or not.

Beside this treatment simulator, the prototype proposes another functionality to help radiologists in their treatment planning. This functionality, that we will detail in the next sections, is based on a method that computes the optimal placement for one or more needle probes in order to burn a maximum volume of the tumor and its margin, while preserving healthy tissue.

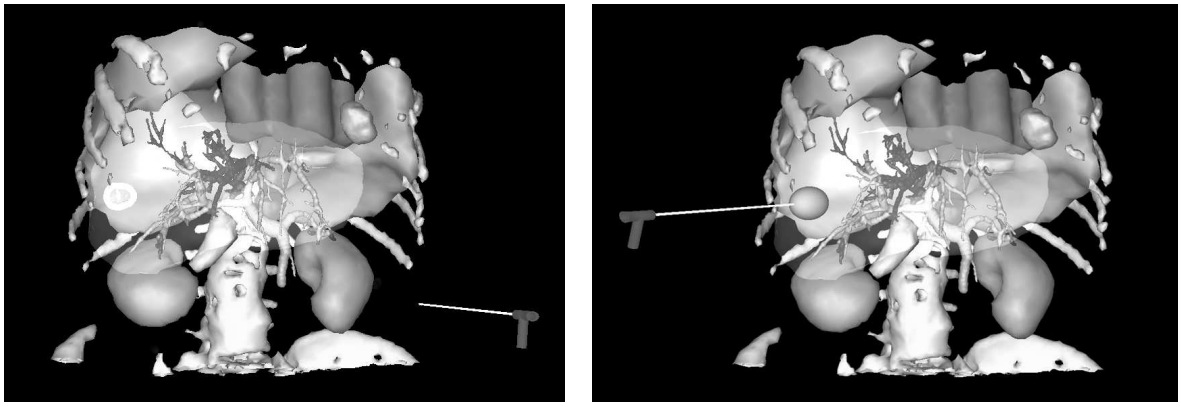

(a) patient's organs and pathology, and an additional virtual probe

(b) estimated necrosis zone corresponding for a specific needle placement

Figure 1. A classic 3d scene with *RF-Sim*

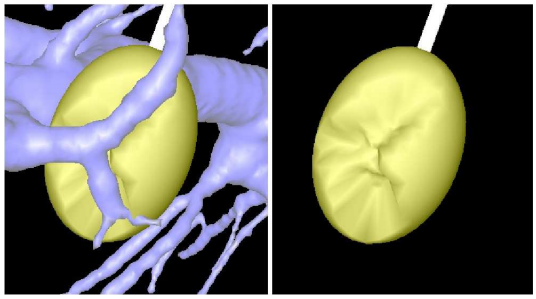

Figure 2. Example of deformation of the necrosis zone due to the presence of vessels. On the right, vessels are hidden to see more clearly the deformation

3.2. Optimal placement of one needle

First, let us examine the case where there is only one tumor, small enough to be treated by a single needle insertion, and where we don't take into account surrounding organs. Then, the problem is reduced to a simpler one: how to find the minimal spheroidal lesion containing the tumor and its margin? This is a classical problem, that can be solved using various possible algorithms of function minimization. If we can dertermine a function finding the smallest spheroid covering the tumor shape knowing a fixed needle axis, then we can try to minimize the value returned by the first function by gradually moving the needle axis, making it quickly converge to a stable minimum. Therefore, our first step is to precisely define the function to minimize.

3.2.1. Volume minimization with fixed needle axis

Let us notice that the lesion shape we consider has particular properties, because of its generation from microholes located at the needle tip, that allow us to make a simplification in the evaluation of its volume. It is a prolate *spheroid*, whose major axis is the needle, *i.e.* an ellipsoid where radii r_1, r_2, and r_3 verify: $r_3 = r_1$ and $r_2 = k.r_1$, and k is the ratio: $\{major\ axis\ size\}$ / $\{minor\ axis\ size\}$. Therefore, the volume of such a spheroid being $V = \frac{4}{3}\pi r_1 r_2 r_3$, it can be rewritten as $V = \frac{4}{3}\pi k r_1^3$.

In this particular case of a single lesion, we consider this simplification: including the margin in the lesion will be seen as including all margin mesh vertices inside the spheroid. Now, given the center C of the ellipsoid and the orientation of its axes, and given the tumor margin mesh, we can define a function that finds the minimum r_1 such that every vertex of the mesh is inside the spheroid. This is done by initializing r_1 to a small value, and then for each vertex of the mesh, increasing r_1 minimally if the vertex was outside so that it comes inside.

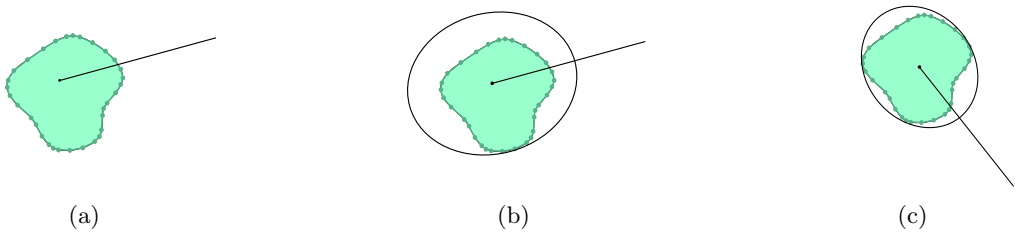

(a) (b) (c)

Figure 3. (a) and (b): fitting an ellipse with fixed center and orientation around a 2D shape; (c): fitting a minimal ellipse around a 2D shape

A point $p(x, y, z)$ is inside the spheroid if and only if $\frac{x^2}{r_1^2} + \frac{y^2}{k^2 r_1^2} + \frac{z^2}{r_1^2} < 1$. So the algorithm is the following. We initialize r_1 to $\sqrt{x_0^2 + \frac{y_0^2}{k^2} + z_0^2}$, considering that the first point $p_0(x_0, y_0, z_0)$ of the mesh is on the initial spheroid. Then, for each vertex p_i of the margin mesh, we test if it is inside the current spheroid or not: if $\frac{x_i^2}{r_1^2} + \frac{y_i^2}{k^2 r_1^2} + \frac{z_i^2}{r_1^2} > 1$, we replace r_1 by $r_1' = \sqrt{x_i^2 + \frac{y_i^2}{k^2} + z_i^2}$. At the end, we obtain the minimal particular spheroid containing all vertices, according to the given center and orientations. This minimal covering volume function will be called *ComputeBestSize*, and be used as our function to minimize. Fig.3(a) and (b) illustrate the application of this algorithm on a 2D example.

3.2.2. Finding the best position for the needle

Now that we can compute the best bounding spheroid around a tumor margin knowing its center and orientation, we have to find the best center and orientation minimizing this bounding volume. We can use one of the classic minimization algorithms (using no derivatives), such as downhill simplex or Powell's direction set methods in multidimensions, or simulated annealing method.[11]

We consider *ComputeBestSize* as taking 6 parameters: 3 center coordinates and 3 orientations of the spheroid. Therefore, we use minimization methods in $n = 6$ dimensions. Downhill simplex method (DH) has to start with an initial simplex X, *i.e.* $n + 1 = 7$ vertices. We use as parameters the initial center $X_0 = (0, 0, 0, 0, 0, 0)$, and a weighting of the 6 unit vectors $X_1 \dots X_6$, as well as a tolerance *tol* determining the termination criterion. After a few iterations, the initial simplex has contracted itself into a valley floor, and is returned by the algorithm: $(X_0(0), X_0(1), X_0(2))$ is an approximation of the best center, and $X_0(3), X_0(4)$, and $X_0(5)$ are approximations of the best orientation coordinates of the spheroid. We can see on Fig.3(c) the minimal fitting ellipse that can be found using this method on the previous 2D example.

In a similar way, Powell's direction set method (PW) needs an initial point $X_0 = (0, 0, 0, 0, 0, 0)$, a set of initial directions $(X_1 \dots X_6)$, and a tolerance *tol*. After some successive line minimizations along coordinate directions, it returns the best point and orientation as X_0 when there is a failure to decrease the function value by more than *tol*. However, both methods have the drawback to be sensitive to local minima. Because of that, we improve the result accuracy by first bringing roughly the needle at an initial position, estimated to be close to the best position, or at least by placing the needle tip inside tumor margin.

To avoid this phenomenon, we tried to use the simulated annealing algorithm, that is less subject to local minima. It is based on random steps, that become smaller and smaller as a factor T decreases. It allows jumps over local hills to find possibly better valleys. However, in our case this method did not give as good results as expected, because of a very long execution time, and because the involved parameters are very difficult to adjust. It would be too long to find the parameters that fit each new tumor shape, each new patient case.

Results of all three methods are exposed in Sec. 4.

3.3. Larger tumors treatments with multiple needle optimal placement

As we said earlier, until now there is a maximum size for lesions because of the limits of RF technology. This limit makes it necessary to itemize large margin meshes in smaller sets that could be covered with smaller overlapping spheroids.

(a) using mesh representation (b) using voxel representation

Figure 4. Trying to cover a 2D shape with 4 ellipses

(a) subsets using distance from needle tips (b) smallest ellipsoids for each subset

Figure 5. Division of a voxel shape in 4 subsets

3.3.1. Using voxel representation of tumors

When using several spheroids to cover a mesh, we can not simplify anymore by only including all mesh's vertices, because in some cases a consequential portion of the mesh volume can be forgotten, as shown on Fig.4(a) in a 2D example.

Therefore, we decided to include the whole voxel representation, as illustrated on Fig.4(b), to ensure a total burning of the shape. However, we will still keep the meshed margin for display. This modification does not affect much execution time, because we deal with structures of a quite reasonable size.

The voxel representation of the security margin is quite easy to obtain, as we already have the tumor voxel representation, that was directly reconstructed from the scans. We only have to perform an enlargement on the tumor voxel shape to obtain the margin voxel shape. To do this, we first perform a *distance transform* on the voxels, to produce a *distance map*, *i.e.* an assignation of a scalar d to each point of the image, d representing the distance from the tumor.[12] Then, we threshold the distance map, according to a margin size s, to add to tumor voxel shape every voxel being at a distance $d < s$ from it. For now, we consider $s = 5mm$ as being the most commonly used margin size, but we allow the user to modify (increase or decrease) this size in a near-real-time operation, simply thresholding the distance with a different value. However, in most cases, this treatment is done once, when the data are loaded.

3.3.2. Modification of *ComputeBestSize*

According to this new representation and the addition of more needles, we modified *ComputeBestSize* to produce a new algorithm called *ComputeBestSizeMoreSpheroids*. Recall that the inputs are fixed needle positions, and that our aim is to find the minimum size for each lesion in order to cover the whole voxel shape.

We first cut the voxel shape in smaller subsets that we will be able to include in lesions of a reasonable size. We distribute the voxels in the subsets, called *influence zones*, according to their distance to needle tips: a point in the tissue will be burnt by the nearest needle. We show an example of the result in 2D on Fig.5(a).

Then, when the distribution is done, we perform the previous algorithm for each needle and its subset, to find the smallest covering spheroid (see Fig.5(b)). The returned volume (to minimize) is the sum of the volumes of the spheroids.

To find the best positions for the needles, we perform one of the optimization algorithms, simply passing as parameters all tip positions and needle orientations, and having the new *ComputeBestSizeMoreSpheroids* algorithm as a value to minimize. After a moment, a convergence, determined by the given tolerance *tol*, fixes all needle positions and orientations.

3.4. Vital structures avoidance

Another important criterion for a successfull RF treatment is the total safety of the procedure. The choice of secure trajectories for needle insertions is an essential point. That is why we decided to include a collision detection system that allows extrahepatic and intrahepatic vital structures avoidance.

In order to take into account surrounding vital or rigid organs, we have to control the optimization process, by preventing the research of the minimum to converge to an unauthorized trajectory. A trajectory is acceptable only if it intersects skin, liver, and a tumor and its margin. All trajectories intersecting other organs are forbidden, either because a needle insertion through them would be fatal, or cause serious damages (heart, portal vein, etc.), or because their physical properties do not allow a needle to go through (bones). Therefore, for each considered trajectory, we need to compute its intersections with the patients organs.

To compute intersections, we use an algorithm based on the voxel representation of the organs. We construct a voxel set from all vital organs that have to be avoided (*i.e.* all organs except skin, liver, tumor and margin). Then this set is enlarged of $5mm$, using mathematic morphology techniques, in order to let a safety margin around it to avoid trajectories involving major risks. This set is then used as a prohibited area, through which the needle can't pass. For each considered trajectory, we compute the intersection with this enlarged set.

Then, we use the result of the collisions detection as a condition to weigh the volume returned by *ComputeBestSizeMoreSpheroids*. If the trajectory is wrong, this function will return such a high volume that the optimization function will necessarily decide to give up progression in this direction and search for a more secure path.

Practically talking, if the needle, for the lesion of which we are going to compute the best size, is going to cross a forbidden organ, then we do not perform the best volume computation, and we place instead as a volume a very high value, prohibitive enough for the optimization process. That way, we save time as many of the tried trajectories will not need a fitting computation, and the time used to compute intersections will be more or less compensated.

4. EXPERIMENTATION DATA AND RESULTS

4.1. Choice of a minimization method

We present on Fig.6 a comparison between results obtained with both methods and different precisions, on a set of 12 patients having a single small liver tumor. All patients' data came from the Strasbourg Civil Hospital and were performed within a preoperative framework. For each case, we launched the method twice.

We chose to compare Downhill simplex (DH) and Powell's direction set (PW) methods with the respective precisions 10^{-3} and 10^{-4} for the first, and 10^{-2} and 10^{-1} for the second, because of their good relevance in terms of ratio *quality of result / execution time*. For both methods, lower or greater precisions gave unacceptable poor quality results or long execution times. On both histograms, whatever the precision, DH method gives better results in almost all cases.

For small tumors, both methods give quite similar volumes. For larger tumors, the difference between volumes is more noticeable, and DH method is better than PW. The average difference between volumes is 2124 mL, but this is mainly caused by the peak of case 7. If we eliminate lowest and largest cases to avoid exceptional values, the average difference becomes 780 mL, and represents an average of 4.53% of the minimum volume (nearly 46% in the worst case).

DH method is also the fastest, especially for large tumors. In 66% of cases, even the slowest DH (10^{-4}) is faster than the fastest PW (10^{-1}). Regarding volume and time performances, DH method being the most interesting, we chose to give preference to DH method, and mainly use it in our further works.

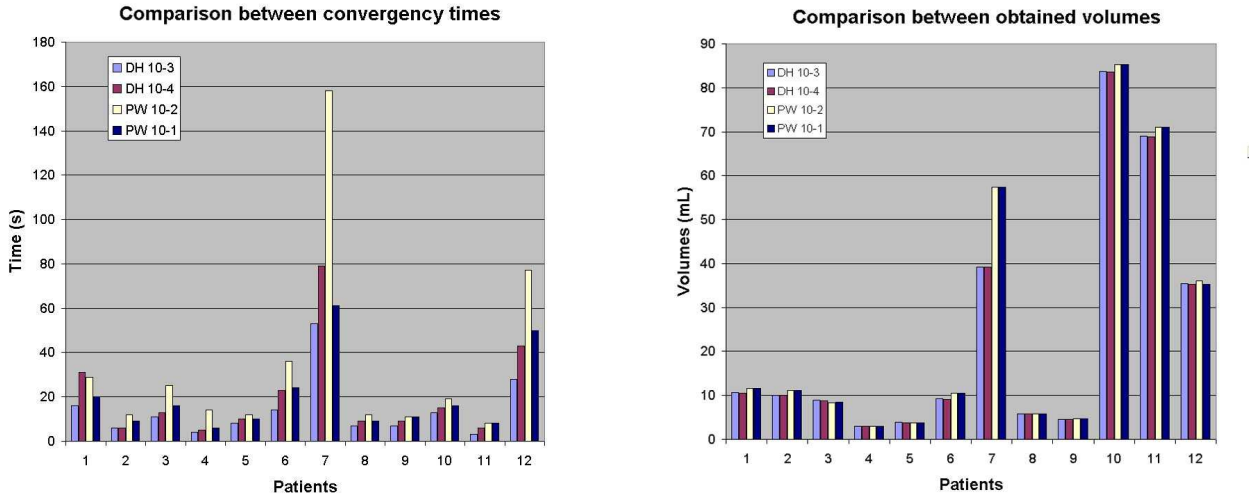

Figure 6. Minimization results

case	tumor(s)		lesion(s)		effic.
nb	nb	volume	nb	volume(s)	of burn
1	1	7.4	1	10.6	69.8%
2	1	6.5	1	10.1	64.3%
3	1	5.2	1	8.8	59.1%
4	1	2.1	1	2.9	72.4%
5	1	3.1	1	3.8	81.6%
6	1	7.1	1	9.2	77.2%

case	tumor(s)		lesion(s)		effic.
nb	nb	volume	nb	volume(s)	of burn
7	1	4.1	1	5.8	70.7%
8	1	3.7	1	4.5	82.2%
9	1	18.7	2	19.9, 17.6	*n.c.*
10	2	6.9	2	3.4, 6.7	68.3%
11	3	48.6	5	13.9, 20.1, 27.7, 24.4, 14.7	*n.c.*
12	6	14.4	6	2.8, 2, 2.1, 2.3, 5.5, 2.3	84.7%

Table 1. Resulting volumes of minimizations (mL)

4.2. Needle placement prediction efficiency

A first set of experiments were carried out on 12 patient cases with liver metastases, whose CT scans were provided by our collaborators at the Strasbourg Civil Hospital. Among these cases, 8 had small single tumors ($< 10mL$), 1 had a large single tumor needing 2 needles, and 3 had multiple tumors (2, 3, and 6 tumors/case). Multiple tumors are considered as one with several connected components, each of them being treated by their nearest needle.

First, automated reconstruction of all patients organs were successfully achieved from enhanced spiral CT scans with 2 mm cuts. Then, an optimal needle(s) placement was obtained in each case, that was confirmed by expert radiologists. Table 1 summarizes the volumes of predicted lesions compared to volumes to burn.

These experiments show an efficiency above 59.1% (of cancerous cells inside burnt zone), with an average of 73%. Related to the various shapes that tumors can have (tumors never fit exactly an ellipsoid), this can be considered as a good result. Some percentages are not filled because the volume of lesions union has not yet been implemented. Fig.7 shows a possible covering of a tumor with 2 minimal lesions, whose placements were found automatically by our prototype.

From the point of view of process duration, obviously the minimization process takes more time as the number of necessary needles increases, and as the size of the tumor is larger (has a great number of voxels). It starts from 1 second (for the smallest tumor of case 4, with an Athlon XP 1800+, 512 Mo RAM), and reaches 6 minutes for the most complicated case (#11). We conclude that, if precision seems to be satisfactory, it would be appreciable to find a less time-consuming optimization of the algorithm.

We are currently waiting for extra data to perform our second set of validation experiments, that would allow us to compare the simulated ablation zones to actual ablation zones based on post-ablation CT scans. It will

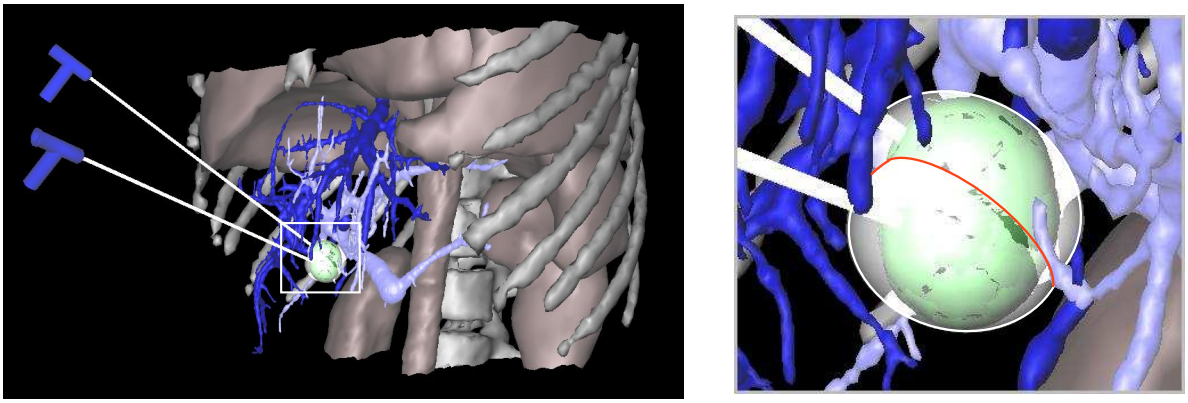

Figure 7. Minimization of the burning zone using 2 overlapping spheroids

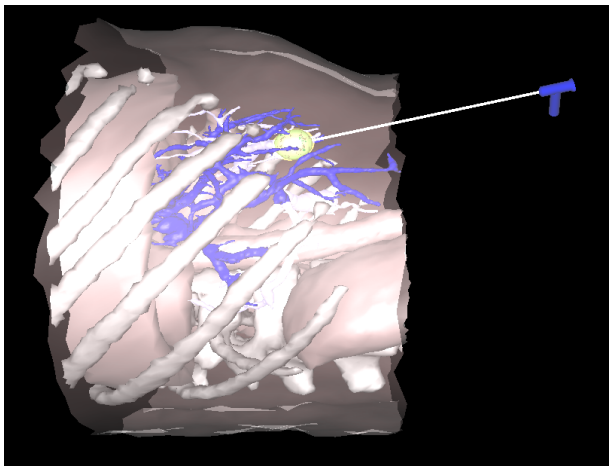

Figure 8. Trajectory impossible to reproduce in practice

consist in a preoperative automatic treatment planning, and then a comparison *a posteriori*, in terms of efficiency and accuracy, with the effective treatment that was performed.

5. DISCUSSION

Now let us examine a few points. First, the collision detection to avoid perforation of other organs is a plus of our system, but may sometimes become a too strong constraint. If the user first places the needle at an approximative position located in a very narrow path through organs, and then launches the optimization process, it may sometimes prevent the process to find a good solution that would be located outside this path, because the converging movements of the needle can't pass through the prohibited area. It will cause the process to find the best placement within this narrow path. For now, the only way to handle this is to try other potential start areas. We are currently studying this problem.

Another current study concerns the way to constraint even more the process, either to respect a need from radiologists to impose a specific entry zone, or to avoid scenarios impossible to reproduce by radiologists (for example, a needle that would be parallel to the body, as shown on Fig.8). For the first case, we added a functionality to the system that allows the radiologist to draw an "insertion window" on the skin (Fig.9), and that forces the system to discover the optimal result within the selected area. This also has the advantage to reduce the field of possible results, and to speed up the process.

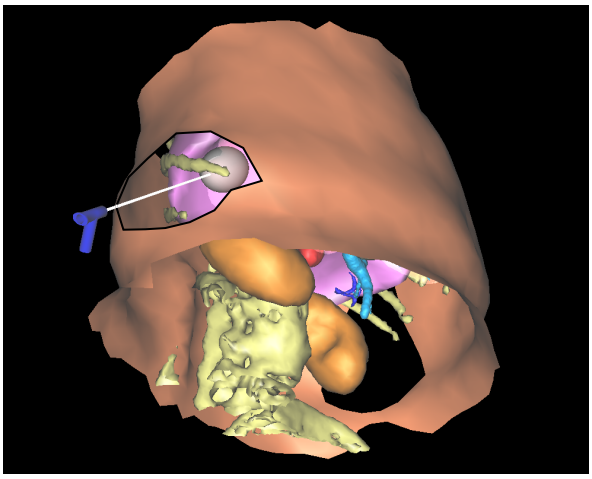

Figure 9. Restriction of the search within a predefined window

For the second case, in a first idea we chose to impose one restriction to the trajectory: it has to cross the skin. That way, we will never obtain such an impossible result. However, it may sometimes be too restrictive: for instance if the scan data contain only a few slices, concerning a small portion of the abdomen, a whole interval of solutions (orientations) may be forgotten. This point is also being studied.

6. CONCLUSION

This experiment confirmed the feasibility of RFA modeling, simulation, and automatic planning. The real-time deformation of the necrosis shape according to local vessels positions, and the automatic placement of the needle with respect to surrounding organs will improve strategic planning and prediction of treatments results. The tool *RF-Sim* also aims to be used for training of novice surgeons, to help them in comparing their strategy proposal to an optimal needle position that would be proposed by the system.

However, for all uses, we plan to improve efficiency of the algorithms to speed up the process and to have a more robust tool able to treat even the most difficult and specific cases. We also plan to enhance our tool with extra radiologic information to increase realism even more.

This system is also planned to be coupled with a haptic device to simulate the force feedback when inserting the needle, and with a virtual reality display system, in order to provide the user with a quality immersive impression, reinforcing the sensation of realism. Some preliminary experiments of manipulation with a haptic device, including organs deformations and force feedback are currently in progress and give very promising results.

ACKNOWLEDGMENTS

The authors would like to thank EPML IRMC* (EPML 9 CNRS-STIC) for its financial support.

REFERENCES

1. J. P. McGahan and G. D. Dodd III, "Radiofrequency ablation of the liver: Current status," *American Journal of Roentgenology* **176**(1), pp. 3–16, 2001.
2. B. Cady, R. L. Jenkins, G. D. Steele Jr., W. D. Lewis, M. D. Stone, W. V. McDermott, J. M. Jessup, A. Bothe, P. Lalor, E. J. Lovett, P. Lavin, and D. C. Linehan, "Surgical margin in hepatic resection for colorectal metastasis: a critical and improvable determinant of outcome," *Annals of Surgery* **227**, pp. 566–571, 1998.

*Equipe-Projet Multi-Laboratoires Imagerie et Robotique Mdicale et Chirurgicale; `http://irmc.u-strasbg.fr/`

3. L. Soler, H. Delingette, G. Malandain, J. Montagnat, N. Ayache, C. Koehl, O. Dourthe, B. Malassagne, M. Smith, D. Mutter, and J. Marescaux, "Fully automatic anatomical, pathological, and functional segmentation from ct scans for hepatic surgery," *Computer Aided Surgery* **6**(3), pp. 131–142, 2001.
4. T. de Baere, A. Denys, B. J. Wood, N. Lassau, M. Kardache, V. Vilgrain, Y. Menu, and A. Roche, "Radiofrequency Liver Ablation: Experimental Comparative Study of Water-Cooled Versus Expandable Systems," *Am. J. Roentgenol.* **176**(1), pp. 187–192, 2001.
5. S. Rossi, F. Garbagnati, R. Lencioni, H.-P. Allgaier, A. Marchiano, F. Fornari, P. Quaretti, G. D. Tolla, C. Ambrosi, V. Mazzaferro, H. E. Blum, and C. Bartolozzi, "Percutaneous Radio-frequency Thermal Ablation of Nonresectable Hepatocellular Carcinoma after Occlusion of Tumor Blood Supply," *Radiology* **217**(1), pp. 119–126, 2000.
6. T. Livraghi, S. N. Goldberg, S. Lazzaroni, F. Meloni, L. Solbiati, and G. S. Gazelle, "Small hepatocellular carcinoma: Treatment with radio-frequency ablation versus ethanol injection," *Radiology* **210**(3), pp. 655–661, 1999.
7. J. C. Rewcastle, G. A. Sandison, P. Kennedy, B. J. Donnelly, and J. C. Saliken, "3-dimensional visualization of simulated prostate cryosurgery," in *Soc. Cardiovascular & Interv. Radiology 25th Ann. Meeting*, San Diego, 2000.
8. S. Tungjitkusolmun, S. Staelin, D. Haemmerich, J.-Z. Tsai, J. G. Webster, F. T. Lee, D. M. Mahvi, and V. R. Vorperian, "Three-dimensional finite element analyses for radio-frequency hepatic tumor ablation," *IEEE Trans. Biomed. Eng.* **49**(2), pp. 3–9, 2002.
9. T. Butz, S. K. Warfield, K. Tuncali, S. G. Silverman, E. van Sonnenberg, F. A. Jolesz, and R. Kikinis, "Pre- and intra-operative planning and simulation of percutaneous tumor ablation," in *proceedings of MICCAI*, *Lecture Notes in Computer Science* **1935**, pp. 317–326, Springer Verlag, 2000.
10. C. Villard, L. Soler, N. Papier, V. Agnus, S. Thery, A. Gangi, D. Mutter, and J. Marescaux, "Virtual radiofrequency ablation of liver tumors," in *proceedings of IS4TM*, *Lecture Notes in Computer Science* **2673**, pp. 366–374, Springer Verlag, 2003.
11. W. H. Press, S. A. Teukolsky, W. T. Vetterling, and B. P. Flannery, *Numerical Recipes in C++: The Art of Scientific Computing (Second Edition)*, Cambridge University Press, 2002.
12. A. Meijster, J. B. T. M. Roerdink, and W. H. Hesselink, "A general algorithm for computing distance transforms in linear time," 2000.